ADVANCING EARTH AND SPACE SCIENCES

JGR Space Physics

RESEARCH ARTICLE

10.1029/2023JA031803

Key Points:

- Plasma density has the greatest impact on electron loss among the tested parameters
- Increasing trend in electron lifetimes with plasma density which becomes more pronounced at higher electron energies
- Results depend crucially on adapted wave normal angle model which represents growth rate profile more consistently than in previous works

Supporting Information:

Supporting Information may be found in the online version of this article.

Correspondence to:

K. Stoll,
katja.stoll@dlr.de

Citation:

Stoll, K., Pick, L., Wang, D., Cao, X., Ni, B., & Shprits, Y. (2023). Variation of electron lifetime due to scattering by electrostatic electron cyclotron harmonic waves in the inner magnetosphere with electron distribution parameters. *Journal of Geophysical Research: Space Physics*, *128*, e2023JA031803. https://doi.org/10.1029/2023JA031803

Received 26 JUN 2023
Accepted 17 NOV 2023

Variation of Electron Lifetime Due To Scattering by Electrostatic Electron Cyclotron Harmonic Waves in the Inner Magnetosphere With Electron Distribution Parameters

Katja Stoll[1,2], Leonie Pick[1], Dedong Wang[3], Xing Cao[4], Binbin Ni[4], and Yuri Shprits[2,3,5]

[1]German Aerospace Center (DLR), Institute for Solar-Terrestrial Physics, Neustrelitz, Germany, [2]Institute of Physics and Astronomy, University of Potsdam, Potsdam, Germany, [3]GFZ German Research Centre for Geosciences, Potsdam, Germany, [4]Department of Space Physics, School of Electronic Information, Wuhan University, Wuhan, China, [5]Department of Earth, Planetary, and Space Sciences, University of California, Los Angeles, Los Angeles, CA, USA

Abstract Through resonant wave-particle interactions with electrostatic electron cyclotron harmonic (ECH) waves, low-energy plasma sheet electrons can be scattered into the atmospheric loss cone and precipitate. This process can be investigated by calculating bounce-averaged quasi-linear diffusion coefficients. However, the numerical calculation of ECH wave-induced scattering rates requires the specification of several parameters, including the properties of the hot plasma sheet electrons responsible for the wave excitation. The dependence of the diffusion coefficients on these parameters and the exact contribution of scattering by ECH waves to diffuse auroral precipitation is still poorly understood and has not been carefully quantified yet. In this study, we calculate bounce-averaged quasi-linear scattering rates and compare the resulting lifetimes to the strong diffusion limit. We vary the temperature, plasma density, and loss cone parameters of the hot component in the electron loss cone distribution over a large range based on previous studies and observations. By adopting a new model that derives the wave normal angle from the midpoint and the angular width of the growth rate profile, our findings suggest that the electron lifetime near the loss cone is not significantly affected by the hot electron temperature and loss cone parameters. However, there is an increase in electron lifetimes with increasing plasma density. For an electric field amplitude of 1 mV/m, the electron lifetime is below or equal to the lifetime calculated using the strong diffusion limit up to $E = 0.25$ keV when $n = 1.5$ cm^{-3}, and up to $E = 0.22$ keV when $n = 9$ cm^{-3}.

1. Introduction

Wave-particle interactions in the Earth's magnetosphere can lead to the scattering of electrons in the central plasma sheet into the atmospheric loss cone. This process is generally associated with the violation of the first and second adiabatic invariants, such that the pitch angle of initially trapped particles approaches the loss cone angle and the particles are lost to the atmosphere, causing the optical phenomenon of diffuse aurora.

Several studies (e.g., Fukizawa et al., 2020, 2022; Horne & Thorne, 2000; Lyons, 1974; Ni, Thorne, Horne, et al., 2011; Ni et al., 2016) suggested that electrostatic electron cyclotron harmonic (ECH) waves can efficiently precipitate plasma sheet electrons at energies of several hundred eV to a few keV and contribute to the formation of the diffuse aurora. While Thorne et al. (2010) concluded that scattering by whistler-mode chorus waves is the dominant cause of diffuse auroral precipitation in the inner magnetosphere at $L < 8$, ECH waves are suggested to be an important and even major driver of the nightside electron diffuse auroral precipitation in the outer magnetosphere (e.g., Ni et al., 2012; Zhang et al., 2015). Furthermore, ECH wave scattering is a possible cause of pulsating aurora (e.g., Liang et al., 2010), and they have recently been suggested to be important for the generation of dayside diffuse aurora (Lou et al., 2021). The exact contribution of the diffusion of low-energy plasma sheet electrons into the atmospheric loss cone due to wave-particle interactions with ECH waves has been a subject of debate. While theoretical calculations of diffusion coefficients by Lyons (1974) suggested that ECH waves had amplitudes large enough to cause strong pitch angle diffusion of electrons with energies up to a few keV, for example, Belmont et al. (1983); Roeder and Koons (1989); Schumaker et al. (1989) concluded that ECH waves are not the principal mechanism scattering low-energy plasma sheet electrons as the amplitudes of observed emissions are insufficient to account for diffuse auroral precipitation. More recent studies (e.g., Ni et al., 2016; Ni, Thorne, Horne, et al., 2011; Tripathi & Singhal, 2009) suggested that the observed wave amplitudes are sufficient to set electrons of several eV up to a few keV on strong diffusion, depending on the geomagnetic activity level. However, the exact role of ECH waves in driving the diffuse auroral precipitation at different spatial locations and under different geomagnetic conditions remains an open question.

ECH waves are electrostatic emissions observed in narrow frequency bands between the harmonics of the electron cyclotron frequency f_{ce} (e.g., Kennel et al., 1970). They are also known as "$n + 1/2$" waves, although the wave frequency is not necessarily centered at $(n + 1/2)f_{ce}$ (Zhou et al., 2017), and as electron Bernstein mode (Bernstein, 1958). Previous observational and statistical studies (e.g., Gough et al., 1979; Meredith et al., 2009; Ni et al., 2017) have shown that ECH waves occur predominantly at the nightside in the MLT interval of 21–06 hr and are confined to the region of $\pm 3°$ around the magnetic equator. Additionally, they are frequently observed in the dayside magnetosphere at latitudes up to 40°, as reported by Lou et al. (2018). Their group velocity is of the order of 10^5 m/s, which is generally smaller than the thermal velocity of the surrounding plasma, and shows a dependence on frequency and wave normal angle (see Supporting Information S1). The parallel group velocity of ECH waves can be of the same order of magnitude or higher than the perpendicular group velocity, but the waves are damped and dissipate in the parallel direction. As damping becomes stronger with decreasing wave normal angle, they propagate nearly perpendicular to the magnetic field (Baumjohann & Treumann, 1996). The most intense ECH waves occur at $L = 5$–9, but moderately strong ECH emissions can still be observed up to $L = 12$ (Zhang et al., 2013), while they generally intensify with increasing geomagnetic activity (Ni, Thorne, Horne, et al., 2011). ECH waves are thought to be excited by the loss cone instability of the ambient plasma sheet electrons (Ashour-Abdalla & Kennel, 1978), although other generation mechanisms like wave-wave interactions between chorus waves and ECH waves (Gao et al., 2018) or the excitation by an electron beam distribution (e.g., Zhang, Angelopoulos, Artemyev, & Zhang, 2021; Zhang, Angelopoulos, Artemyev, Zhang, & Liu, 2021) are possible.

In general, the waves can resonate with particles when the Doppler-shifted wave frequency experienced by the particle equals a multiple of the electron cyclotron frequency. In order to solve the resonance condition and find the velocities and energies of the particles that the wave will interact with, we need to know the cyclotron frequency, wave frequency and wave propagation angle and we must solve the plasma dispersion relation relating the wave frequency to the wave vector. Therefore, information about the wave propagation characteristics and the specification of the spatial distribution of the background magnetic field and plasma density and properties of the hot plasma sheet electrons responsible for the wave excitation, such as temperature and loss cone parameters, is required. Lou et al. (2022) performed a sensitivity analysis of ECH wave-induced scattering rates to the ambient magnetic field intensity, total electron density, and density ratio between hot and cold electrons, finding that the variation of the parameters can significantly change the magnitude of the diffusion coefficients of electrons with energies <1 keV. In this study, we aim to extend these results by investigating the sensitivity of previously unexplored properties of the hot electron component to constrain the conditions under which ECH wave-induced scattering can theoretically make a significant contribution to the total diffuse auroral precipitation. This information is relevant to practice because it helps to decide whether this precipitation mechanism (ECH-wave induced scattering driven by loss cone instability) needs to be considered under what conditions (i.e., parameters of the electron distribution) when analyzing actual precipitation events. Additionally, resonant interactions between particles and ECH waves have an impact on electron phase space density evolution, but typical quasilinear studies of radiation belt dynamics do not currently incorporate them. This is because the resonant electron energy due to ECH waves is typically less than 10 keV, which is much lower than the energy range of radiation belt electrons. However, there are recent results by Haas et al. (2023), suggesting that it might be important to consider ECH waves in ring current models. Furthermore, to our knowledge, a comprehensive statistical model of waves that includes the wave normal angle as well as the electron loss cone distribution parameters, which are responsible for wave excitation, has yet to be developed.

We calculate bounce-averaged quasi-linear scattering rates due to ECH waves and analyze the dependence on the temperature, plasma density and loss cone parameters of the hot electron component in the electron distribution. In Section 2, we present our methods used to calculate the ECH wave-induced diffusion coefficients and the underlying assumptions about the wave properties and the background plasma. The numerical results of the diffusion coefficients and electron lifetimes for different electron distributions are shown in Section 3, and are discussed in Section 4 and summarized in Section 5.

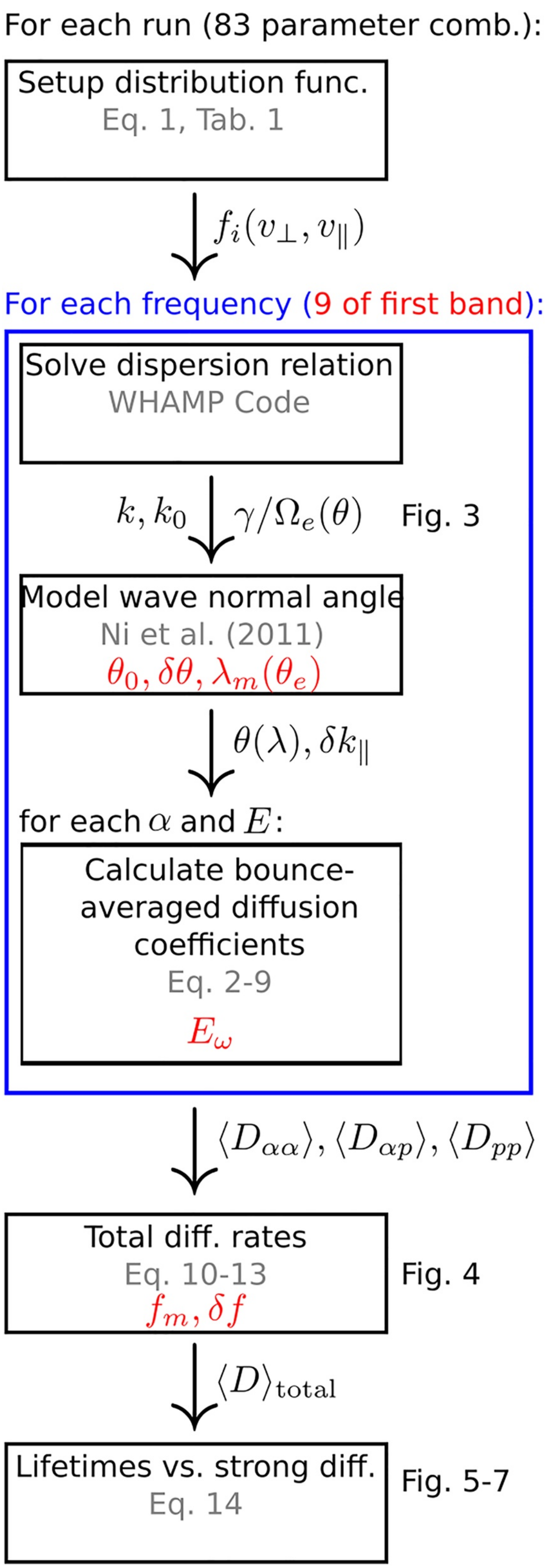

Figure 1. Full Diffusion Code for the calculation of quasi-linear bounce-averaged diffusion coefficients for wave-particle interaction with ECH waves. The core calculation block of the code is indicated in blue and assumptions to be discussed are highlighted in red.

2. Methods and Assumptions

2.1. Initial Electron Distribution

Figure 1 gives an overview of the different steps involved in the calculation of the bounce-averaged quasi-linear scattering rates due to ECH waves, indicating the main input and output of each step.

Following previous studies (e.g., Lou et al., 2022; Ni et al., 2012; Ni, Thorne, Horne, et al., 2011), we assume that the electron distribution can be modeled by a sum of subtracted bi-Maxwellian components, each given by (Ashour-Abdalla & Kennel, 1978)

$$f_i(v_\perp, v_\parallel) = \frac{n_i}{\pi^{3/2} a_{\perp,i}^2 a_{\parallel,i}} \exp\left(-\frac{v_\parallel^2}{a_{\parallel,i}^2}\right) \cdot \left\{ \Delta_i \exp\left(-\frac{v_\perp^2}{a_{\perp,i}^2}\right) + \frac{1-\Delta_i}{1-\beta_i} \left[\exp\left(-\frac{v_\perp^2}{a_{\perp,i}^2}\right) - \exp\left(-\frac{v_\perp^2}{\beta_i a_{\perp,i}^2}\right) \right] \right\}, \tag{1}$$

where n_i is the electron density, $a_{\perp,i}$ and $a_{\parallel,i}$ are the thermal velocities perpendicular and parallel to the ambient magnetic field and Δ_i and β_i are the loss cone parameters determining the filling and the slope of the distribution inside the loss cone. The thermal velocities are related to the parallel and perpendicular temperatures of the plasma by $a_{\parallel,i}^2 = 2T_{\parallel,i}/m_e$ and $a_{\perp,i}^2 = 2T_{\perp,i}/m_e$, where m_e is the electron mass. Figure 2 shows a plot of the distribution given by Equation 1 for different values of Δ and β corresponding to the two extreme cases of maximum and minimum influence of the loss cone term. When $\Delta = 1$, the distribution reduces to a simple Maxwellian distribution without loss cone term. For $\Delta = 0$ and $\beta = 0.99$, the influence of the loss cone term in Equation 1 maximizes and the phase space density becomes zero for small values of $v_\perp$, corresponding to no particles inside the loss cone.

We assume the electron distribution to consist of one cold, isotropic component and one hot component including a loss cone. The parameters adopted in the distribution are listed in Table 1 and represent typical conditions in the plasma sheet at around $L = 6$, following previous studies (Fukizawa et al., 2020; Horne & Thorne, 2000; Lou et al., 2022; Ni, Thorne, Horne, et al., 2011). The temperature of the cold and hot electrons is 1 eV (Horne & Thorne, 2000; Lou et al., 2022) and 621 eV, respectively. The loss cone parameters of the hot component are set to $\beta = 0.02$ and $\Delta = 0.5$ (Horne & Thorne, 2000; Lou et al., 2022). The total electron density is adopted from the plasma trough density model in Sheeley et al. (2001) and the density ratio between hot and cold electrons is set to be 1/2. The background magnetic field intensity is assumed to be $B_0 = 143$ nT, representing the dipole magnetic field intensity at $L = 6$. We vary the hot electron temperature T_h, plasma density n and loss cone parameters Δ and β choosing 20 values of $T_\perp$, $T_\parallel$, Δ and β, respectively, and three different values for n within the range indicated in Table 1, which is based on the parameters obtained in previous studies based on observations (e.g., Fukizawa et al., 2020; Ni, Thorne, Horne, et al., 2011; Zhou et al., 2017).

2.2. Frequency-Dependent Diffusion Coefficients

This subsection refers to the steps in the blue box in Figure 1. The parameters listed in Table 1 can be used as input to the WHAMP (Waves in homogeneous, anisotropic, multicomponent plasmas) Code (Roennmark, 1982) to solve the hot plasma dispersion relation for nine specific frequencies in the

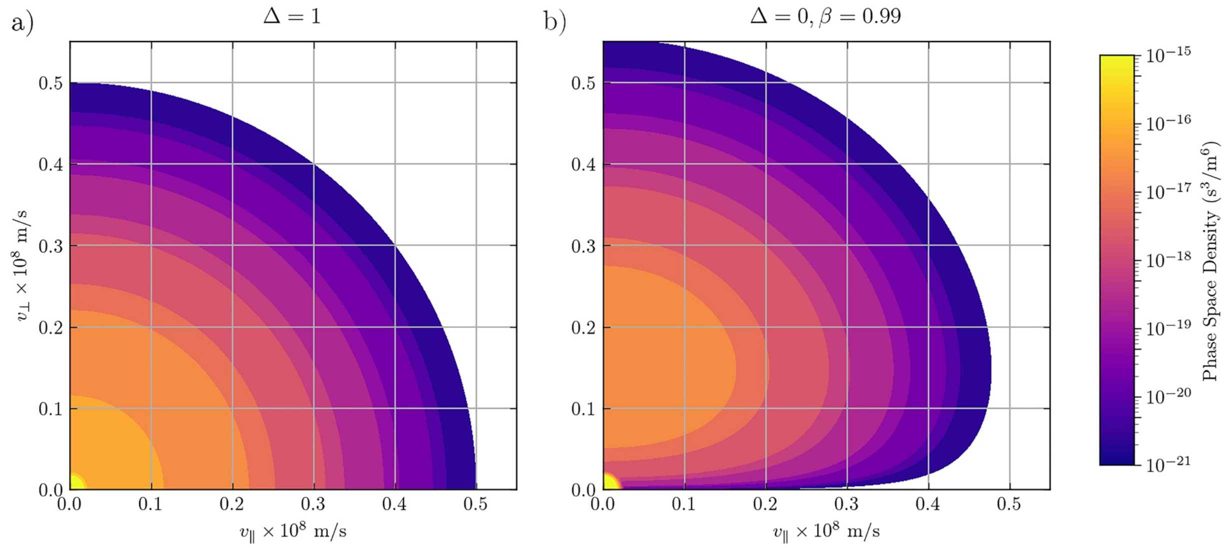

Figure 2. (a) Loss cone distribution in ($v_\perp$, $v_\parallel$)-space as described by Equation 1 for $\Delta = 1$, corresponding to a bi-Maxwellian distribution, and (b) for $\Delta = 0$ and $\beta = 0.99$, showing the maximum influence of the loss cone term.

first harmonic band, from $f = 1.1$ f_{ce} to $f = 1.9$ f_{ce} with a step of $f = 0.1$ f_{ce}. For each frequency, we vary the wave normal angle θ between 86° and 89.96°. In Figure 3, the distributions of the wave growth rate with wave normal angle computed with WHAMP are shown for ten different hot electron temperatures and for three different plasma densities at $f = 1.3$ f_{ce}. The growth rate is normalized to the angular electron gyrofrequency $\Omega_e = |eB_0/m_e|$ and its maximum value varies between $\gamma/\Omega_e \sim 10^{-7}$ and $\gamma/\Omega_e \sim 10^{-3}$ depending on frequency and on the electron distribution described above. We see that the growth rate maximum generally tends to decrease as $T_\parallel = T_\perp$, $T_\perp/T_\parallel$, Δ and β increase. The values of the growth rate maximum correspond to timescales of ~0.25 s to ~42 min of the considered instability. For reference, this is comparable to or greater than the bounce time of the considered electrons, which varies between ~11 s (for $E = 1$ keV) and ~36 s (for $E = 100$ eV).

Following Ni, Thorne, Horne, et al. (2011), we define the model of the wave normal angle distribution by the wave normal angle θ_0, the width $\delta\theta$, perpendicular and parallel components of the wave number $k_\perp$ and $k_\parallel$, and the spread in the parallel wave number $\delta k_\parallel$. As the growth rate remains almost constant over a range of wave normal angles (Figure 3), we select the midpoint of this plateau as the wave normal angle θ_0 and define the width as $\delta\theta = 90° - \theta_0$. We adopt the model for the latitudinal variation of the wave normal angle from Ni, Thorne, Horne, et al. (2011). For each frequency, θ_0 is taken as the equatorial wave normal angle θ_e and depending on that value, it is assumed that the wave can propagate up to $\lambda_m = 1°$ (if $\theta_e \geq 89.8°$), 2° (if $89.5° \leq \theta_e < 89.8°$) or 3° (if $\theta_e < 89.5°$) in latitude. The relation between wave normal angle and latitude is assumed to be linear, so that $\theta = a \cdot \lambda + \theta_e$ with a slope a, which depends on $\lambda_m = [1°, 2°, 3°]$ so that $\theta(\lambda_m) = 90°$. We linearly interpolate the wave normal angle between ($\lambda = 0°$, $\theta = \theta_0 = \theta_e$) and ($\lambda = \lambda_m$, $\theta = 90°$). By combining the results from WHAMP with the wave normal angle model, the latitudinal variation of the wave normal angle θ, the width $\delta\theta = 90° - \theta$, parallel and perpendicular wave number $k_\parallel$ and $k_\perp$ and the spread in the parallel wave number $\delta k_\parallel = k_{\perp,0}/\tan(\theta - \delta\theta) - k_{\parallel,0}$ are obtained, where $k_{0,\perp} = k_0 \cdot \sin\theta_0$ and $k_{0,\parallel} = k_0 \cdot \cos\theta_0$ are the perpendicular and parallel components of the wave

Table 1
Electron Components Used to Model the Electron Distribution Function Consisting of One Cold and One Hot Component Including a Loss Cone

Parameter	$T_\perp$ (eV)	$T_\parallel$ (eV)	n (m^{-3})	Δ	β
Comp. 1 (cold)	1	1	3.31×10^6	1	–
Comp. 2 (hot)	621	621	1.65×10^6	0.5	0.02
Variation of comp. 1	–	–	1×10^6 to 6×10^6	–	–
Variation of comp. 2	100 to 10,000	100 to 10,000	0.5×10^6 to 3×10^6	0.3 to 0.9	0.01 to 0.4

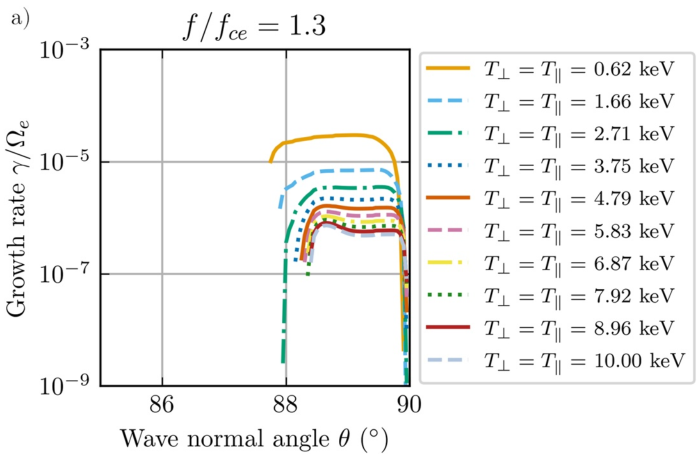

Figure 3. (a) Normalized growth rate as a function of wave normal angle for $f = 1.3$ f˙ce for ten different hot electron temperatures and (b) for three different plasma densities.

vector k_0 corresponding to θ_0. These parameters can be used further to calculate bounce-averaged quasi-linear diffusion coefficients.

The local pitch angle diffusion coefficients due to electrostatic ECH waves are given by (e.g., Horne & Thorne, 2000; Lyons, 1974)

$$D_{\alpha\alpha} = \sum_{n=-\infty}^{\infty} \int k_\perp \, dk_\perp \left[\Psi_{n,k} \left(\frac{n\Omega_e/\omega_k - \sin^2\alpha}{\sin\alpha\cos\,\alpha} \right)^2 \right]_{k_\parallel = k_{\parallel,res}},$$
$$\Psi_{n,k} = \frac{1}{4\pi} \frac{e^2}{m_e^2} \frac{|E_k|^2}{V} \left(\frac{\omega_k}{|k|} \right)^2 \frac{J_n^2(k_\perp v_\perp/\Omega_e)}{v^4 |v_\parallel - \partial\omega_k/\partial k_\parallel|}, \tag{2}$$

where α is the electron pitch angle, $k_{\parallel,res} = (\omega_k - n\Omega_e/\gamma)/v_\parallel$ is the resonant parallel wave number, ω_k is the wave frequency as a function of k, γ is the Lorentz factor, and J_n is the Bessel function of order n. Horne and Thorne (2000) developed Equation 2 into a modified version,

$$D_{\alpha\alpha} = \frac{\sqrt{\pi}}{2} \frac{e^2}{m_e^2} \frac{|E_w|^2}{k_{0,\perp}^2 \delta k_\parallel} \frac{\exp(-\mu)}{v^5 \cos\,\alpha}$$
$$\cdot \sum_{n=-\infty}^{+\infty} \left(\frac{n\Omega_e/\omega_k - \sin^2\alpha}{\sin\,\alpha\,\cos\,\alpha} \right)^2 I_n(\mu) \left\{ \exp\left[-(\zeta_n^-)^2\right] + \exp\left[-(\zeta_n^+)^2\right] \right\}, \tag{3}$$

where $I_n(\mu)$ is the modified Bessel function of order n with the argument $\mu = k_{0,\perp} v_\perp^2 / (2\Omega_e^2)$, and $\zeta_n^\pm = \frac{\omega_k - n\Omega_e}{\delta k_\parallel v \cos\,\alpha} \pm \frac{k_{0,\parallel}}{\delta k_\parallel}$. This can be done under the assumption of an electric field spectrum of the form

$$|E_k|^2 = C' k_\perp^2 \exp\left[-\left(\frac{k_\perp}{k_{0,\perp}} \right)^2 \right] \cdot \left\{ \exp\left[-\left(\frac{k_\parallel - k_{0,\parallel}}{\delta k_\parallel} \right)^2 \right] + \exp\left[-\left(\frac{k_\parallel + k_{0,\parallel}}{\delta k_\parallel} \right)^2 \right] \right\} \tag{4}$$

with a normalization constant

$$C' = \frac{4\pi^{3/2}}{k_{0,\perp}^4 \delta k_\parallel} V |E_w|^2. \tag{5}$$

here, E_w is the wave amplitude, and V is the plasma volume. Furthermore, it is assumed that the parallel group velocity is small compared to the electron parallel velocity (i.e. $\partial\omega_k/\partial k_\parallel \ll v_\parallel$, see Supporting Information S1).

The local mixed diffusion rates $D_{\alpha p}$ and momentum diffusion rates D_{pp} can subsequently be obtained by

$$D_{\alpha p} = D_{\alpha\alpha} \left[\frac{\sin\alpha\cos\,\alpha}{n\Omega_e/(\gamma\omega_k) - \sin^2\alpha} \right] \qquad D_{pp} = D_{\alpha\alpha} \left[\frac{\sin\alpha\cos\,\alpha}{n\Omega_e/(\gamma\omega_k) - \sin^2\alpha} \right]^2, \tag{6}$$

10.1029/2023JA031803

and the quasi-linear bounce-averaged diffusion coefficients are calculated by (e.g., Glauert & Horne, 2005; Shprits, Thorne, et al., 2006; Summers et al., 2007)

$$\langle D_{\alpha\alpha}\rangle = \frac{1}{S(\alpha_{eq})}\int_0^{\lambda_m} D_{\alpha\alpha}(\alpha)\frac{\cos\alpha}{\cos^2\alpha_{eq}}\cos^7\lambda\,\mathrm{d}\lambda, \tag{7}$$

$$\langle D_{\alpha p}\rangle = \frac{1}{S(\alpha_{eq})}\int_0^{\lambda_m} D_{\alpha p}(\alpha)\frac{\cos^4\lambda\left(1+3\sin^2\lambda\right)^{1/4}}{\cos\alpha}\,\mathrm{d}\lambda, \tag{8}$$

$$\langle D_{pp}\rangle = \frac{1}{S(\alpha_{eq})}\int_0^{\lambda_m} D_{pp}(\alpha)\frac{\cos\lambda\left(1+3\sin^3\lambda\right)^{1/2}}{\cos\alpha}\,\mathrm{d}\lambda, \tag{9}$$

where $S(\alpha_{eq})$ gives the variation of the electron bounce period τ_B with the equatorial pitch angle α_{eq}, approximated by $S(\alpha_{eq}) = 1.3 - 0.56\sin\alpha_{eq}$ in a dipole magnetic field (Hamlin et al., 1961). α_{eq} is associated with the local pitch angle by $\sin^2\alpha = \frac{\sqrt{4-3\cos^2\lambda}}{\cos^6\lambda}\sin^2\alpha_{eq}$. λ_m is the upper limit of the magnetic latitude determined either by the mirror latitude of the particles or by the maximum latitude of the wave occurrence obtained from the wave normal angle model.

We calculate bounce-averaged diffusion coefficients as given in Equations 7–9 for 200 values of the equatorial pitch angle ranging from $\alpha_{eq} = 0°$ to $\alpha_{eq} = 90°$ and for 201 values of the electron kinetic energy ranging from $E = 0.01$ keV to $E = 100$ keV.

2.3. Total Diffusion Coefficients

Given that the wave electric field and wave normal angle distribution are known, the bounce-averaged resonant diffusion coefficients can be evaluated for ECH waves at the nine specified frequencies. Theoretically, the quantification of diffusion rates requires an integration over the entire ECH frequency band, which depends on solving the hot plasma dispersion relation. Ni, Thorne, Horne, et al. (2011) have developed an approximate method instead, using the observed ECH wave power spectrum to introduce weighting factors for the diffusion rates at each wave frequency. The overall bounce-averaged diffusion rates due to the nine frequencies in the first harmonic band are computed by

$$\langle D\rangle_{\text{total}} = \sum_{j=1}^{9} R_j\langle D\rangle_j \tag{10}$$

with the weighting factor for the jth wave frequency given by

$$R_j = \frac{(I_E)_j}{\sum_{j=1}^{9}(I_E)_j}. \tag{11}$$

here, $\langle D\rangle_j$ is the bounce-averaged diffusion rate due to the jth wave frequency and $(I_E)_j$ is the electric field intensity for the jth wave frequency, given by

$$(I_E(f))_j = A\exp\left[-\left(\frac{f_j - f_m}{\Delta f}\right)^2\right], \quad (f_{lc} < f < f_{uc}) \tag{12}$$

when assuming a Gaussian frequency distribution, with f_m and Δf being the frequency of maximum wave power and bandwidth, respectively, and f_{lc} and f_{uc} being the lower and upper cutoffs to the wave spectrum outside which the wave power is assumed to be zero. A is a normalization factor given by

$$A = \frac{E_w^2}{\Delta f}\frac{1}{\pi^{3/2}}\left[\mathrm{erf}\left(\frac{f_m - f_{lc}}{\Delta f}\right) + \mathrm{erf}\left(\frac{f_{uc} - f_m}{\Delta f}\right)\right]^{-1}, \tag{13}$$

where E_w is the wave electric field amplitude.

Following previous studies (e.g., Horne & Thorne, 2000; Lou et al., 2022), we assume a nominal wave amplitude of $E_w = 1$ mV/m and consider only the first harmonic band of ECH emissions, that is, $f_{ce} < f < 2f_{ce}$, which is the

10.1029/2023JA031803

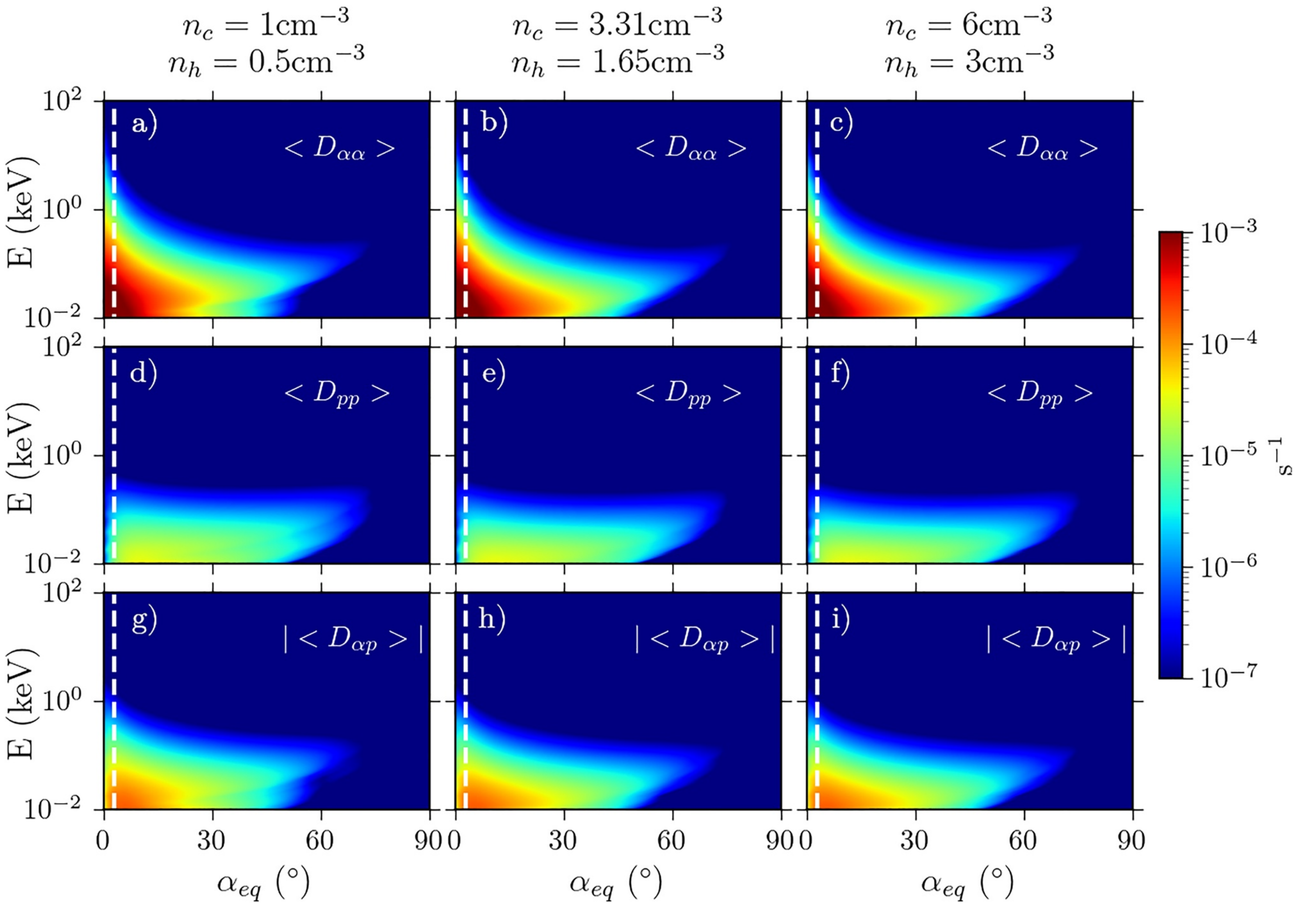

Figure 4. (a)–(c) Quasi-linear bounce-averaged pitch angle diffusion coefficients $\langle D_{\alpha\alpha}\rangle$, (d)–(f) momentum diffusion coefficients $\langle D_{pp}\rangle$ and (g)–(i) mixed diffusion coefficients $|\langle D_{\alpha p}\rangle|$ as a function of equatorial pitch angle α_{eq} and electron kinetic energy E for three different plasma densities $n = 1.5$ cm^{-3} (left column), $n = 4.96$ cm^{-3} (middle column) and $n = 9$ cm^{-3} (right column). The white dashed line indicates the loss cone angle α_{LC}.

strongest compared to the other bands (Ni et al., 2017; Ni, Thorne, Horne, et al., 2011; Roeder & Koons, 1989) and contributes most to the scattering rates near the loss cone (see Text S2 in Supporting Information S1). Based on the statistical results from Ni et al. (2017), we assume that the wave power is centered at $f_m = 1.4$ f$_{ce}$ and that the bandwidth is $\Delta f = 0.2$ f$_{ce}$. Thus, we calculate bounce-averaged quasi-linear diffusion coefficients at the nine specified frequencies, including contributions from the Landau resonance ($n = 0$) and the cyclotron resonances from $n = -10$ to $n = 10$, and apply the weighting with the wave power spectral profile as described above in order to obtain total diffusion rates from the first harmonic band.

3. Model Results

In Figure 4, we show examples of the two-dimensional bounce-averaged pitch angle diffusion coefficients $\langle D_{\alpha\alpha}\rangle$, momentum diffusion coefficients $\langle D_{pp}\rangle$ and mixed diffusion coefficients $|\langle D_{\alpha p}\rangle|$ as a function of equatorial pitch angle α_{eq} and electron kinetic energy E for three different plasma densities. From the upper panels, it can be inferred that ECH waves can efficiently scatter electrons in pitch angle in the energy range from less than 0.1 keV to approximately 1 keV over a broad range of pitch angles from 0° to ~60°. At higher energies >1 keV, the range of pitch angles for which efficient scattering in pitch angle can occur narrows significantly, suggesting that ECH waves play a negligible role in scattering plasma sheet electrons at these energies. With increasing plasma density, the resonant pitch angle range changes slightly at low energies, extending to larger pitch angles and lower energies for a higher plasma density. Compared to pitch angle diffusion, the momentum diffusion, shown in Figures 4d to 4f, is several orders of magnitude weaker. The same applies for the mixed diffusion rates, shown in Figures 4g to 4i.

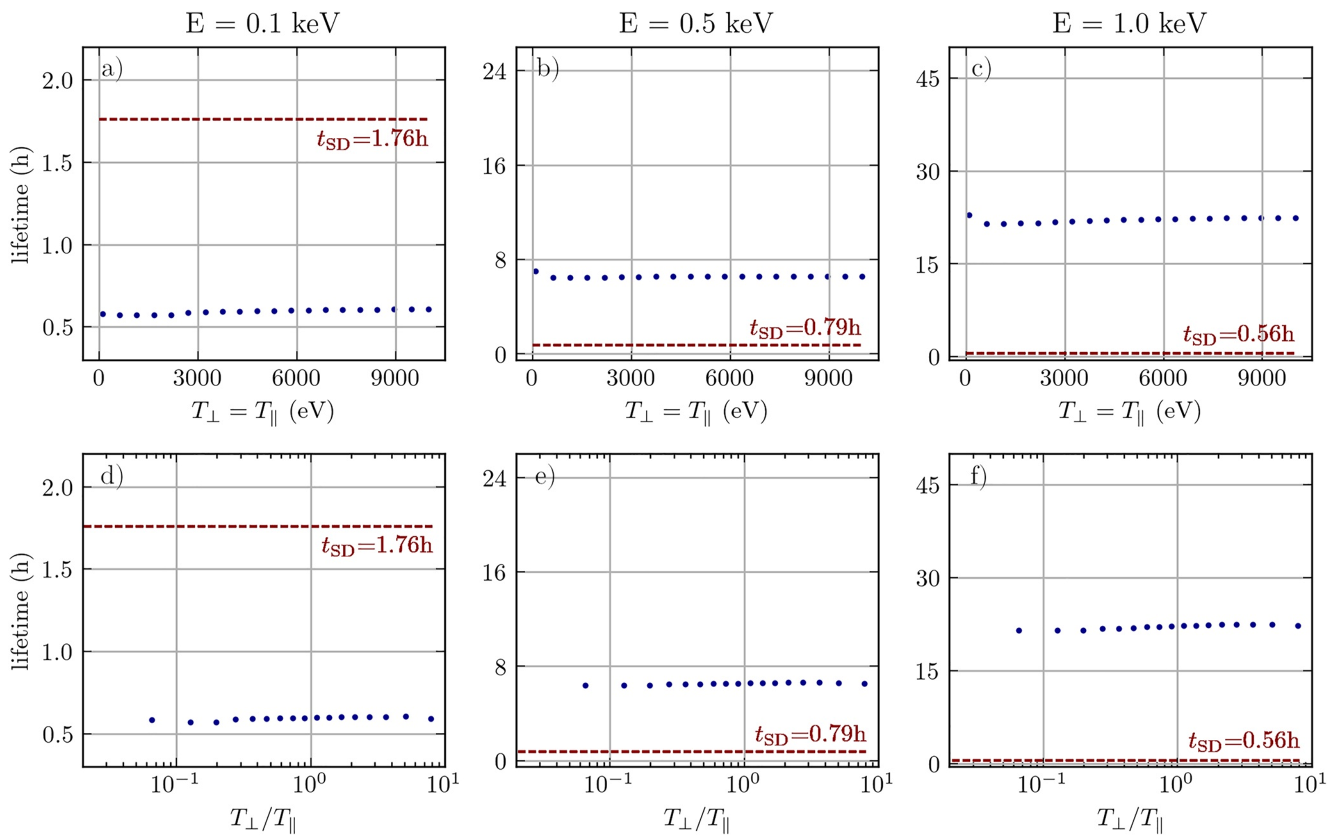

Figure 5. Electron lifetimes near the loss cone for three different energies ($E = 0.1$ keV, $E = 0.5$ keV and $E = 1$ keV from left to right) (a)–(c) as a function of hot electron temperature when $T_\perp = T_\parallel$ and (d)–(f) for increasing temperature anisotropy $T_\perp/T_\parallel$. The lifetime of strong diffusion at the corresponding electron energy is indicated by the red dashed line.

In order to investigate the contribution of ECH waves to the diffuse auroral precipitation, we calculate the lifetime of electrons near the loss cone and compare it to the strong diffusion limit. Lifetime is a relevant parameter because it describes the timescale on which the particle distribution would go to an equilibrium state due to the wave-particle interactions (e.g., Shprits, Li, & Thorne, 2006; Albert & Shprits, 2009) and is important for including the scattering due to ECH waves into numerical codes solving the diffusion equation and simulating the dynamics of the ring current, for example, Following Shprits, Li, and Thorne (2006), we estimate the electron loss timescale as $1/\langle D_{\alpha\alpha}\rangle|_{LC}$, where the bounce-averaged pitch angle diffusion coefficient $\langle D_{\alpha\alpha}\rangle$ is evaluated at the equatorial loss cone angle α_{LC}. Assuming a dipolar magnetic field, we find that $\alpha_{LC} = 2.85°$ at $L = 6$. Following Summers and Thorne (2003), the strong diffusion rate is approximated by

$$D_{SD} \approx \frac{9.66}{L^4}\left[\frac{4L}{4L-3}\right]^{1/2}\frac{\left[E'(E'+2)\right]^{1/2}}{(E'+1)} \tag{14}$$

for electrons of a specified kinetic energy in units of their rest energy $E' = E/(m_e c^2)$ at $L = 6$, and the lifetime of strong diffusion is obtained by $t_{SD} = 1/D_{SD}$.

The resulting electron loss times and lifetimes of strong diffusion are shown in Figure 5 for three specific electron energies $E = 0.1$ keV, $E = 0.5$ keV and $E = 1$ keV. For each energy, we plot the electron lifetime near the loss cone as a function of hot electron temperature with $T_\perp = T_\parallel$ and as a function of temperature anisotropy $T_\perp/T_\parallel$. For $E = 0.1$ keV, the loss timescale is about 35 min (about 60 times larger than the bounce time of the considered electrons), which is below the strong diffusion limit of $t_{SD} = 1.76$ hr, and remains nearly constant within an interval of about 2 min if $T_\perp = T_\parallel$ and for the considered values of temperature anisotropy. We therefore expect ECH waves to be able to fully fill the loss cone and dominate diffuse auroral precipitation at this electron energy. For $E = 0.5$ keV, the calculated lifetimes are about 6.8 hr, while the strong diffusion limit decreases to $t_{SD} = 0.79$ hr.

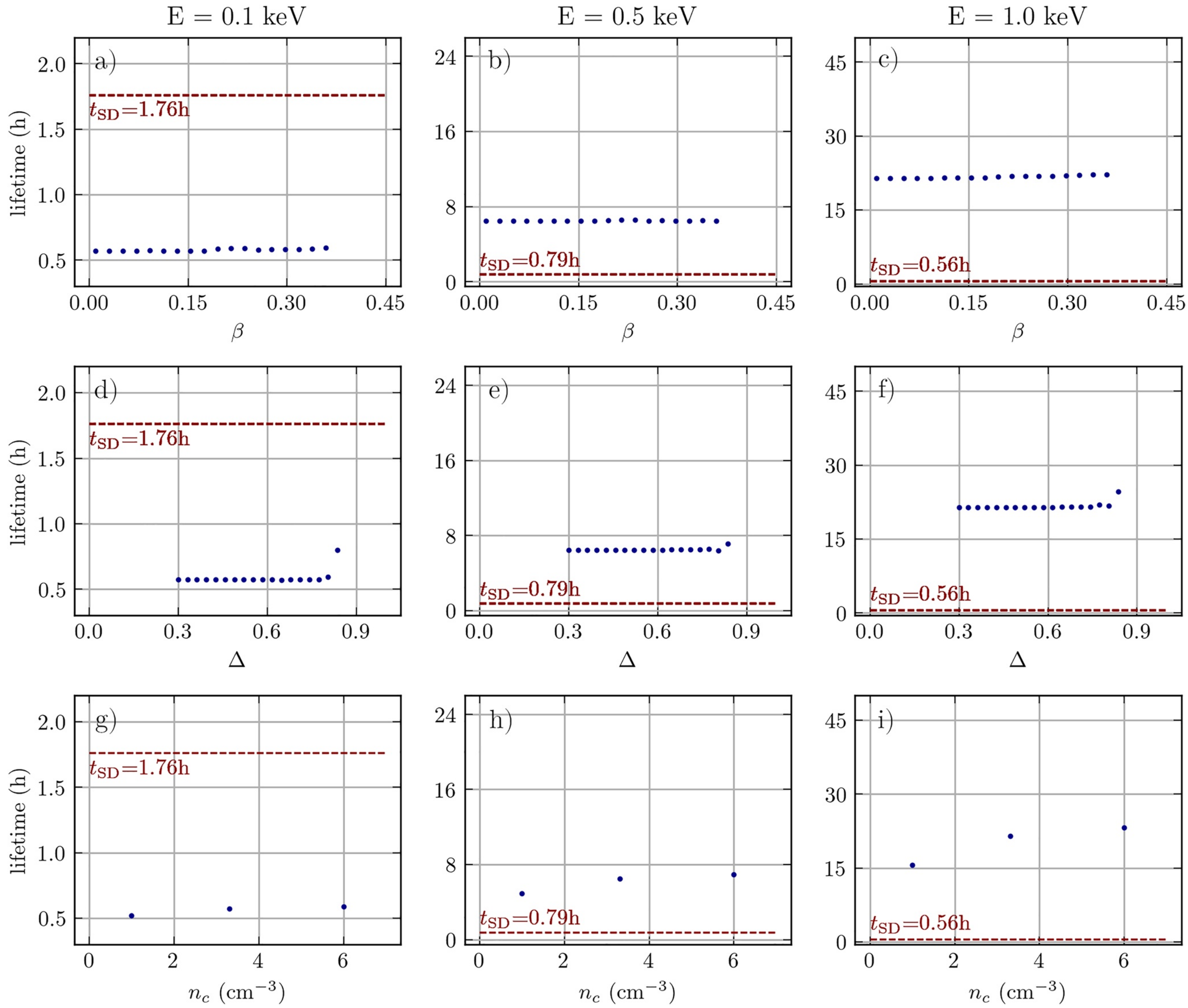

Figure 6. Electron lifetimes near the loss cone for three different energies ($E = 0.1$ keV, $E = 0.5$ keV and $E = 1$ keV from left to right) (a)–(c) as a function of loss cone parameters β and (d)–(f) Δ and (g)–(i) cold plasma density. The lifetime of strong diffusion at the corresponding electron energy is indicated by the red dashed line.

For $E = 1$ keV, the lifetime increases to close to a day, while the strong diffusion limit drops to approximately 30 min. Our results therefore show that ECH waves can importantly contribute to diffuse auroral precipitation of electrons with energies of several hundreds of eV, while diffusion by ECH waves is not important for electrons with higher energies $E > 1$ keV under the assumed conditions.

In Figure 6, we show the variation of the electron lifetime near the loss cone with the initial loss cone parameters β and Δ and with the plasma density. Varying β and Δ, the resulting lifetimes do not change by more than 2 min for $E = 0.1$ keV, 5 min for $E = 0.5$ keV and 35 min for $E = 1.0$ keV over a large range of parameters. As Δ increases and approaches $\Delta = 1$, which would mean that the loss cone is completely filled and the distribution in Equation 1 reduces to a stable Maxwellian, the magnitude of the pitch angle diffusion coefficients decreases significantly and the electron lifetime near the loss cone increases correspondingly. Calculating the electron loss timescale for three different values of the total plasma density, while keeping the ratio of hot to cold plasma density constant at $n_h/n_c = 1/2$, we find that the electron loss is enhanced when the plasma density is low. This effect becomes more pronounced with increasing electron energy. The lifetime of electrons near the loss cone increases from 15.6 to 23.2 hr at $E = 1$ keV, when the plasma density increases from $n = 1.5$ to $n = 9$ cm^{-3}. It should be noted that this is not consistent with the results from Lou et al. (2022), who report stronger scattering in case of higher plasma

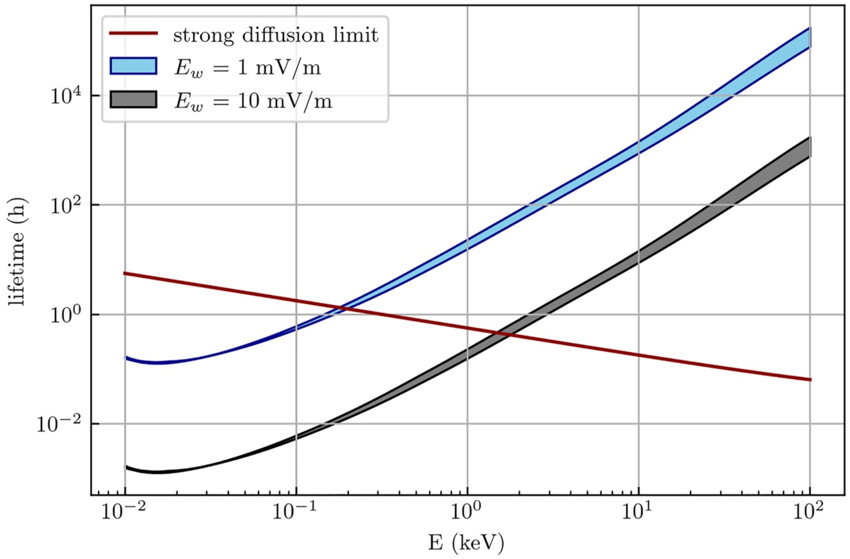

Figure 7. Electron lifetime near the loss cone as a function of energy for two different wave electric field amplitudes. Results are shown for the maximum and minimum lifetimes corresponding to the lowest and highest total electron density, indicating the range of variation of electron lifetimes with varying parameters in the initial electron distribution. The lifetime of strong diffusion is indicated by the red line.

density. Lou et al. (2022) assume the wave growth rate to be centered at a wave normal angle of 89.5° with an angular width of 0.5°, which remains constant with changing plasma density. In our calculations, we see however that the profile of growth rate with wave normal angle changes with plasma density, as shown in Figure 3. This implies different values of the equatorial wave normal angle and angular width for the different plasma densities. As the diffusion coefficients are very sensitive to the wave normal angle (e.g., Horne & Thorne, 2000; Ni, Thorne, Horne, et al., 2011), the changes in wave normal angle lead to the differences in the calculated lifetimes with changing plasma density.

Furthermore, we investigate the effect of the wave electric field amplitude on the scattering efficiency and calculate the range of variation of the lifetime with changing plasma density for each amplitude, calculated for $L = 6$. As shown in Figure 7, electrons can be lost very fast in case of strong ECH wave events with $E_w = 10$ mV/m. The resulting lifetimes remain below or close to the strong diffusion limit up to electron energies of a few keV. In the case considered above with $E_w = 1$ mV/m, the lifetime of electrons with $E = 1$ keV is about two orders of magnitudes higher than the strong diffusion limit and increases further with increasing electron energy. As argued above, the lifetime increases with increasing plasma density. This effect becomes more pronounced with higher electron energies. For example, at $E = 2$ keV, when $E_w = 10$ mV/m, the lifetime varies between $t = 31$ min for $n = 1.5$ cm^{-3} and $t = 48$ min for $n = 9$ cm^{-3} compared to a strong diffusion limit of $t_{SD} = 24$ min. When $E_w = 1$ mV/m, the lifetime varies between $t = 52$ hr for $n = 1.5$ cm^{-3} and $t = 80$ hr for $n = 9$ cm^{-3} for $E = 2$ keV electrons, significantly exceeding the lifetime calculated using the strong diffusion limit. We therefore expect ECH waves to importantly contribute to diffuse auroral precipitation of low-energy electrons of several hundreds of eV, and additionally be able to precipitate higher energy electrons during strong events significantly exceeding wave amplitudes of 1 mV/m.

4. Discussion

As shown in Figure 3, the profile of the growth rate as a function of wave normal angle changes with varying hot electron temperature. While the growth rate remains approximately constant over a range of wave normal angles from 88° to close to 90° for low energetic electron temperatures $T_h < 3$ keV, the distribution shifts to higher wave normal angles and establishes a peak at around 88.6° when the temperature increases. In previous studies (e.g., Horne & Thorne, 2000; Lou et al., 2022), it is assumed that the wave growth is centered at a constant wave normal angle θ determining $k_{0,\perp}$ and $k_{0,\parallel}$ with a constant angular width $\delta\theta$ determining the spread in parallel wave number $\delta k_\parallel$. Ni, Thorne, Horne, et al. (2011) and Lou et al. (2021) on the other hand, use the wave normal angle at the peak of the growth rate θ_0 for the determination of $k_{0,\perp}$ and $k_{0,\parallel}$ and assume a width of $\delta\theta = 90° - \theta_0$. In our calculations, the peak of the growth rate changes significantly with varying hot electron temperature, which would result in changing assumptions for the wave normal angle and width used for calculating the wave vector. This would imply large changes of the pitch angle diffusion coefficients and lifetimes near the loss cone (not shown here). As the calculated growth rates shown in Figure 3 do not establish a clear peak but remain almost constant over a range of wave normal angles, adopting the approach of deriving the equatorial wave normal angle from the peak of the growth rate would have lead to an overestimation of the influence of hot electron temperature on the scattering by ECH waves. Following the approach by for example, Horne and Thorne (2000) on the other hand and assuming a constant wave normal angle for all distributions would lead to an underestimation of the influence of temperature. Our approach of taking the midpoint of the plateau reflects the change in the growth rate profile, but does not result in unrealistically large changes of the wave normal angle distribution and resulting wave vectors. However, the effect of the energetic electron temperature might still be underestimated, as we do not capture the entire profile of the wave normal angle distribution. It might be a better approach to implement a Gaussian distribution of wave normal angles as commonly adopted for chorus waves (e.g., Glauert & Horne, 2005; Ni, Thorne, Meredith, et al., 2011; Ni et al., 2008; Shprits & Ni, 2009). This would however require the transformation of the integral over $k_\perp$ in Equation 2 to an integral over wave normal angle. As shown by Tripathi and Singhal (2009), this transformation involves several terms that must be evaluated using the dispersion relation for ECH waves, and is beyond the scope of this paper.

In studies of ECH wave events, the electron distribution of the form in Equation 1 is usually fitted to the observed phase space density (e.g., Fukizawa et al., 2020; Lou et al., 2021; Ni, Thorne, Horne, et al., 2011). In these event studies, the distribution used to fit the observations usually consists of one cold and five or more hot components. Here, following other theoretical studies (e.g., Horne & Thorne, 2000; Lou et al., 2022), we assume an electron distribution consisting of one cold and one hot component in order to be able to isolate the effect of the different parameters in the hot component. It is not clear how the number of included hot components affects the results of the ECH wave-induced diffusion coefficients.

Additionally, the amplitude of the wave electric field has an important effect on the scattering rates, as $D_{\alpha\alpha} \propto |E_w|^2$. Our results show that during strong wave events when $E_w = 10$ mV/m, pitch angle scattering by ECH waves can contribute significantly to diffuse auroral precipitation of electrons with energies up to a few keV. This is consistent with the results from Fukizawa et al. (2022), who showed that the pitch angle diffusion coefficient for ECH waves can exceed the strong diffusion level up to electron energies of around 2 keV if $E_w = 10$ mV/m. However, Ni et al. (2017) gave statistical average values of the ECH wave amplitude not exceeding 1 mV/m based on THEMIS FFF wave data sets. It is therefore unclear how frequently such strong events with $E_w > 1$ mV/m occur.

Besides the amplitude, the distribution of wave power with frequency plays an important role in evaluating the wave-induced scattering efficiency. While in some studies (e.g., Fukizawa et al., 2022) it was assumed that the wave power spectrum is centered at $(n + 1/2)f_{ce}$, Zhou et al. (2017) reported two ECH emission events where the wave power and wave growth rates are peaked at the lower half interval of harmonic bands between nf_{ce} and $(n + 1/2)f_{ce}$ for one event, but at the upper half interval between $(n + 1/2)f_{ce}$ and $(n + 1)f_{ce}$ for the second event. They found that the peak frequencies of the wave growth rate increase with increasing energetic electron temperature, suggesting that this parameter has an important effect on the wave power spectrum. In our calculations, the growth rate peaks high in the band approaching the high gyroharmonic frequency. Because this is not quite consistent with the observations by Ni et al. (2017), we assume the wave power to be centered at $1.4f_{ce}$ and adopt the weighting method from Ni, Thorne, Horne, et al. (2011). This way, we may however underestimate the influence of the energetic electron temperature on the distribution of wave power with frequency. More detailed wave statistical studies should be a subject of future research.

5. Conclusions

In this study, we have calculated bounce-averaged quasi-linear scattering rates $\langle D_{\alpha\alpha}\rangle$, $\langle D_{pp}\rangle$, and $|\langle D_{\alpha p}\rangle|$, and electron lifetimes near the loss cone for wave-particle interactions with electrostatic ECH waves, varying the temperature of the energetic electron component $T_\parallel$ and $T_\perp$, loss cone parameters β and Δ, and the plasma density n in the electron loss cone distribution. Our main conclusions are summarized as follows:

1. ECH waves predominantly interact with electrons of energies of a few hundreds of eV, leading to pitch angle scattering into the loss cone and consequently diffuse auroral precipitation. The electron lifetimes are

comparable to the lifetimes calculated using the strong diffusion limit up to approximately 300 eV when $E_w = 1$ mV/m and up to about 2 keV when $E_w = 10$ mV/m, and increase with increasing energy. This is consistent with the results obtained by Tripathi and Singhal (2009), who found that ECH waves are responsible for diffuse auroral precipitation of electrons with energies of a few hundred eV. Also consistent with previous studies (e.g., Ni, Thorne, Horne, et al., 2011; Thorne et al., 2010), we find that the effect of momentum diffusion due to ECH wave scattering is minor.

2. The electron lifetimes remain almost unaffected by the energetic electron temperature, regardless of whether the thermal velocity distribution is isotropic or anisotropic. The same applies to changing loss cone parameters β and Δ, except when Δ becomes close to 1, where we observe a significant increase in lifetime. Furthermore, the plasma density has an important effect on the pitch angle scattering rates, leading to a shorter loss timescale for low plasma densities. This effect becomes more pronounced with increasing electron energy. For example, the lifetime of electrons near the loss cone increases from $t = 15.6$ hr to $t = 23.2$ hr at $E = 1$ keV, and from $t = 52$ hr to $t = 80$ hr at $E = 2$ keV, when the plasma density increases from $n = 1.5$ cm^{-3} to $n = 9$ cm^{-3}.
3. We find that the growth rate remains approximately constant over a range of wave normal angles between 88° and 90°, depending on the parameters in the electron loss cone distribution, instead of establishing a clear peak. Due to the considerable dependence of the scattering rates on the wave normal angle, we adapt the retrieval of the wave normal angle from the midpoint and the angular width of the growth rate profile. This approach reflects major changes in the growth rate profile with the tested parameters without overestimating their influence.

Besides the influence of the hot electron temperature, loss cone parameters and plasma density, the dependence of the scattering rates on the wave normal angle distribution remains to be explored in more detail. Our results suggest that the energetic electron temperature can alter the profile of wave growth rate as a function of wave normal angle. Currently, the wave normal angle distribution is modeled by a peak or midpoint wave normal angle determining $k_{0,\perp}$ and $k_{0,\|}$ and an angular width $\delta\theta$ determining the spread in parallel wave number $\delta k_{\|}$. However, this cannot capture all changes in the profile. In addition, Zhou et al. (2017) suggested that the energetic electron temperature has an effect on the wave power spectrum and in particular on the location of the center of the ECH wave spectrum in the harmonic band. Therefore, detailed knowledge of the wave power spectrum as well as the wave normal angle distribution could improve the calculations of ECH wave-induced scattering effects. Furthermore, we modeled the electron lifetimes based on the scattering rates near the edge of the loss cone. As the scattering rates drop significantly when $\alpha_{eq} > 60°$, additional scattering by other types of waves, for example, chorus waves, may be needed to scatter electrons at all values of equatorial pitch angles in order to account for diffuse auroral precipitation.

Data Availability Statement

The WHAMP Code (Roennmark, 1982) used in this study is available at https://github.com/irfu/whamp. Numerical output data can be obtained from https://doi.org/10.5281/zenodo.8082305 (available under the Creative Commons Attribution 4.0 International license), Stoll et al. (2023). Data analysis and visualization was performed using the Python packages numpy (Harris et al., 2020), pandas (McKinney, 2010), matplotlib (Hunter, 2007) and pylustrator (Gerum, 2020).

Acknowledgments
Xing Cao acknowledges support from the NSFC Grant 42241143. Dedong Wang acknowledges the support from the DFG Grant–WA 4323/5-1. The authors are grateful for the valuable feedback provided by the two reviewers. Open Access funding enabled and organized by Projekt DEAL.

References

Albert, J. M., & Shprits, Y. Y. (2009). Estimates of lifetimes against pitch angle diffusion. *Journal of Atmospheric and Solar-Terrestrial Physics*, *71*(16), 1647–1652. https://doi.org/10.1016/j.jastp.2008.07.004

Ashour-Abdalla, M., & Kennel, C. F. (1978). Nonconvective and convective electron cyclotron harmonic instabilities. *Journal of Geophysical Research*, *83*(A4), 1531–1543. https://doi.org/10.1029/JA083iA04p01531

Baumjohann, W., & Treumann, R. A. (1996). Basic space plasma physics. https://doi.org/10.1142/p015

Belmont, G., Fontaine, D., & Canu, P. (1983). Are equatorial electron cyclotron waves responsible for diffuse auroral electron precipitation? *Journal of Geophysical Research*, *88*(A11), 9163–9170. https://doi.org/10.1029/ja088ia11p09163

Bernstein, I. B. (1958). Waves in a plasma in a magnetic field. *Physics Reviews*, *109*(1), 10–21. https://doi.org/10.1103/PhysRev.109.10

Fukizawa, M., Sakanoi, T., Miyoshi, Y., Kazama, Y., Katoh, Y., Kasahara, Y., et al. (2022). Statistical study of approaching strong diffusion of low-energy electrons by chorus and ECH waves based on in situ observations. *Journal of Geophysical Research*, *127*(3), e30269. https://doi.org/10.1029/2022JA030269

Fukizawa, M., Sakanoi, T., Miyoshi, Y., Kazama, Y., Katoh, Y., Kasahara, Y., et al. (2020). Pitch-angle scattering of inner magnetospheric electrons caused by ECH waves obtained with the arase satellite. *Geophysical Research Letters*, *47*(23), e89926. https://doi.org/10.1029/2020GL089926

Gao, Z., Su, Z., Xiao, F., Summers, D., Liu, N., Zheng, H., et al. (2018). Nonlinear coupling between whistler-mode chorus and electron cyclotron harmonic waves in the magnetosphere. *Geophysical Research Letters*, *45*(23), 12685–12693. https://doi.org/10.1029/2018GL080635

Gerum, R. (2020). pylustrator: Code generation for reproducible figures for publication. *Journal of Open Source Software*, *5*(51), 1989. https://doi.org/10.21105/joss.01989

Glauert, S., & Horne, R. (2005). Calculation of pitch angle and energy diffusion coefficients with the PADIE code. *Journal of Geophysical Research*, *110*(A4), A04206. https://doi.org/10.1029/2004JA010851

Gough, M. P., Christiansen, P. J., Martelli, G., & Gershuny, E. J. (1979). Interaction of electrostatic waves with warm electrons at the geomagnetic equator. *Nature*, *279*(5713), 515–517. https://doi.org/10.1038/279515a0

Haas, B., Shprits, Y. Y., Allison, H. J., Wutzig, M., & Wang, D. (2023). A missing dusk-side loss process in the terrestrial electron ring current. *Scientific Reports*, *13*(1), 970. https://doi.org/10.1038/s41598-023-28093-2

Hamlin, D. A., Karplus, R., Vik, R. C., & Watson, K. M. (1961). Mirror and azimuthal drift frequencies for geomagnetically trapped particles. *Journal of Geophysical Research*, *66*(1), 1–4. https://doi.org/10.1029/JZ066i001p00001

Harris, C. R., Millman, K. J., van der Walt, S. J., Gommers, R., Virtanen, P., Cournapeau, D., et al. (2020). Array programming with NumPy. *Nature*, *585*(7825), 357–362. https://doi.org/10.1038/s41586-020-2649-2

Horne, R., & Thorne, R. (2000). Electron pitch angle diffusion by electrostatic electron cyclotron harmonic waves: The origin of pancake distributions. *Journal of Geophysical Research*, *105*(A3), 5391–5402. https://doi.org/10.1029/1999JA900447

Hunter, J. D. (2007). Matplotlib: A 2d graphics environment. *Computing in Science & Engineering*, *9*(3), 90–95. https://doi.org/10.1109/MCSE.2007.55

Kennel, C. F., Scarf, F. L., Fredricks, R. W., McGehee, J. H., & Coroniti, F. V. (1970). VLF electric field observations in the magnetosphere. *Journal of Geophysical Research*, *75*(31), 6136–6152. https://doi.org/10.1029/JA075i031p06136

Liang, J., Uritsky, V., Donovan, E., Ni, B., Spanswick, E., Trondsen, T., et al. (2010). THEMIS observations of electron cyclotron harmonic emissions, ULF waves, and pulsating auroras. *Journal of Geophysical Research*, *115*(A10), A10235. https://doi.org/10.1029/2009JA015148

Lou, Y., Cao, X., Ni, B., Tu, W., Gu, X., Fu, S., et al. (2021). Diffuse auroral electron scattering by electrostatic electron cyclotron harmonic waves in the dayside magnetosphere. *Geophysical Research Letters*, *48*(5), e92208. https://doi.org/10.1029/2020GL092208

Lou, Y., Cao, X., Wu, M., Ni, B., & Zhang, T. (2022). Parametric sensitivity of electron scattering effects by electrostatic electron cyclotron harmonic waves. *Journal of Geophysical Research*, *127*, e2022JA030322. https://doi.org/10.1029/2022ja030322

Lou, Y., Gu, X., Summers, D., Ni, B., Liu, K., Fu, S., et al. (2018). Statistical distributions of dayside ECH waves observed by MMS. *Geophysical Research Letters*, *45*(23), 12730–12738. https://doi.org/10.1029/2018GL080125

Lyons, L. R. (1974). Electron diffusion driven by magnetospheric electrostatic waves. *Journal of Geophysical Research*, *79*(4), 575–580. https://doi.org/10.1029/JA079i004p00575

McKinney, W. (2010). Data structures for statistical computing in python. In *Proceedings of the 9th python in science conference* (Vol. 445, pp.51–56).

Meredith, N. P., Horne, R. B., Thorne, R. M., & Anderson, R. R. (2009). Survey of upper band chorus and ECH waves: Implications for the diffuse aurora. *Journal of Geophysical Research*, *114*(A7), A07218. https://doi.org/10.1029/2009ja014230

Ni, B., Gu, X., Fu, S., Xiang, Z., & Lou, Y. (2017). A statistical survey of electrostatic electron cyclotron harmonic waves based on THEMIS FFF wave data. *Journal of Geophysical Research*, *122*(3), 3342–3353. https://doi.org/10.1002/2016ja023433

Ni, B., Liang, J., Thorne, R. M., Angelopoulos, V., Horne, R. B., Kubyshkina, M., et al. (2012). Efficient diffuse auroral electron scattering by electrostatic electron cyclotron harmonic waves in the outer magnetosphere: A detailed case study. *Journal of Geophysical Research*, *117*(A1), A01218. https://doi.org/10.1029/2011JA017095

Ni, B., Thorne, R., Horne, R., Meredith, N., Shprits, Y., Chen, L., & Li, W. (2011). Resonant scattering of plasma sheet electrons leading to diffuse auroral precipitation: 1. Evaluation for electrostatic electron cyclotron harmonic waves. *Journal of Geophysical Research*, *116*(A4), A04218. https://doi.org/10.1029/2010ja016232

Ni, B., Thorne, R., Meredith, N., Horne, R., & Shprits, Y. (2011). Resonant scattering of plasma sheet electrons leading to diffuse auroral precipitation: 2. Evaluation for whistler mode chorus waves. *Journal of Geophysical Research*, *116*(A4), A04219. https://doi.org/10.1029/2010ja016233

Ni, B., Thorne, R., Shprits, Y., & Bortnik, J. (2008). Resonant scattering of plasma sheet electrons by whistler-mode chorus: Contribution to diffuse auroral precipitation. *Geophysical Research Letters*, *35*, L11106. https://doi.org/10.1029/2008gl034032

Ni, B., Thorne, R., Zhang, X., Bortnik, J., Pu, Z., Xie, L., et al. (2016). Origins of the earth's diffuse auroral precipitation. *Space Science Reviews*, *200*(1–4), 205–259. https://doi.org/10.1007/s11214-016-0234-7

Roeder, J. L., & Koons, H. C. (1989). A survey of electron cyclotron waves in the magnetosphere and the diffuse auroral electron precipitation. *Journal of Geophysical Research*, *94*(A3), 2529–2541. https://doi.org/10.1029/ja094ia03p02529

Roennmark, K. (1982). Waves in homogeneous, anisotropic multicomponent plasmas (WHAMP).

Schumaker, T. L., Gussenhoven, M. S., Hardy, D. A., & Carovillano, R. L. (1989). The relationship between diffuse auroral and plasma sheet electron distributions near local midnight. *Journal of Geophysical Research*, *94*(A8), 10061–10078. https://doi.org/10.1029/ja094ia08p10061

Sheeley, B. W., Moldwin, M. B., Rassoul, H. K., & Anderson, R. R. (2001). An empirical plasmasphere and trough density model: CRRES observations. *Journal of Geophysical Research*, *106*(A11), 25631–25642. https://doi.org/10.1029/2000JA000286

Shprits, Y. Y., & Ni, B. (2009). Dependence of the quasi-linear scattering rates on the wave normal distribution of chorus waves. *Journal of Geophysical Research*, *114*, A11205. https://doi.org/10.1029/2009ja014223

Shprits, Y. Y., Li, W., & Thorne, R. M. (2006). Controlling effect of the pitch angle scattering rates near the edge of the loss cone on electron lifetimes. *Journal of Geophysical Research*, *111*(A12), A12206. https://doi.org/10.1029/2006JA011758

Shprits, Y. Y., Thorne, R. M., Horne, R. B., & Summers, D. (2006). Bounce-averaged diffusion coefficients for field-aligned chorus waves. *Journal of Geophysical Research*, *111*(A10), A10225. https://doi.org/10.1029/2006JA011725

Stoll, K., Pick, L., Wang, D., Cao, X., Ni, B., & Shprits, Y. (2023). Variation of electron lifetime due to scattering by electrostatic electron cyclotron harmonic waves in the inner magnetosphere with electron distribution parameters [Dataset]. Zenodo. https://doi.org/10.5281/zenodo.8082305

Summers, D., Ni, B., & Meredith, N. P. (2007). Timescales for radiation belt electron acceleration and loss due to resonant wave-particle interactions: 1. Theory. *Journal of Geophysical Research*, *112*(A4), A04206. https://doi.org/10.1029/2006JA011801

Summers, D., & Thorne, R. M. (2003). Relativistic electron pitch-angle scattering by electromagnetic ion cyclotron waves during geomagnetic storms. *Journal of Geophysical Research*, *108*(A4), 1143. https://doi.org/10.1029/2002JA009489

Thorne, R., Ni, B., Tao, X., Horne, R., & Meredith, N. (2010). Scattering by chorus waves as the dominant cause of diffuse auroral precipitation. *Nature*, *467*(7318), 943–946. https://doi.org/10.1038/nature09467

Tripathi, A. K., & Singhal, R. P. (2009). Diffusion coefficients from resonant interactions with electrostatic electron cyclotron harmonic waves. *Physics of Plasmas*, *16*(11), 112107. https://doi.org/10.1063/1.3264735

Zhang, X., Angelopoulos, V., Artemyev, A. V., & Zhang, X.-J. (2021). Beam-driven ECH waves: A parametric study. *Physics of Plasmas*, *28*(7), 072902. https://doi.org/10.1063/5.0053187

10.1029/2023JA031803

Zhang, X., Angelopoulos, V., Artemyev, A. V., Zhang, X.-J., & Liu, J. (2021). Beam driven electron cyclotron harmonic waves in Earth's magnetotail. *Journal of Geophysical Research*, *126*(3), e28743. https://doi.org/10.1029/2020JA028743

Zhang, X., Angelopoulos, V., Ni, B., & Thorne, R. (2015). Predominance of ECH wave contribution to diffuse aurora in Earth's outer magnetosphere. *Journal of Geophysical Research*, *120*(1), 295–309. https://doi.org/10.1002/2014ja020455

Zhang, X., Angelopoulos, V., Ni, B., Thorne, R., & Horne, R. (2013). Quasi-steady, marginally unstable electron cyclotron harmonic wave amplitudes. *Journal of Geophysical Research*, *118*(6), 3165–3172. https://doi.org/10.1002/jgra.50319

Zhou, Q., Xiao, F., Yang, C., Liu, S., He, Y., Baker, D. N., et al. (2017). Generation of lower and upper bands of electrostatic electron cyclotron harmonic waves in the Van Allen radiation belts. *Geophysical Research Letters*, *44*(11), 5251–5258. https://doi.org/10.1002/2017GL073051